NASA Technical Paper 2897

1989

Mixed Formulation for Frictionless Contact Problems

Ahmed K. Noor
and Kyun O. Kim
The George Washington University
Joint Institute for Advancement of Flight Sciences
Langley Research Center
Hampton, Virginia

National Aeronautics and Space Administration
Office of Management
Scientific and Technical Information Division

Contents

Introduction

Considerable work has been done in recent years on the development of contact algorithms for use in conjunction with finite element programs. These activities were motivated by a variety of practical applications including investigation of wear resistance of machine elements in contact, determination of the load distribution in joints, and determination of the footprint area of tires. Recent work on this subject is reviewed by Kikuchi and Oden (1988); Noor and Tanner (1988); Simo, Wriggers, and Taylor (1985); Torstenfelt (1983); and Wriggers, Wagner, and Stein (1987).

Contact algorithms first used in finite element applications were based on semiempirical approaches such as the gap element approach (see, for example, Stadter and Weiss 1979). These approaches often lacked the generality needed for handling complicated practical problems. Since contact conditions are formulated as inequality constraints, mathematical programming approaches were naturally used to incorporate the contact constraints into the global finite element equations. The two most commonly used methods in this category are the Lagrange multiplier technique and the penalty method (see, for example, Felippa 1978; Kalker 1986; and Kikuchi and Song 1981). The main drawbacks of the Lagrange multiplier technique are that it results in an increase in the number of algebraic equations to be solved and the presence of zero terms along the main diagonal of the coefficient matrix of these equations. In the penalty method the contact conditions are only approximately satisfied and the resulting algebraic equations become ill-conditioned for large values of the penalty parameter.

More recently, a perturbed Lagrangian formulation was proposed for the solution of contact problems. The formulation includes the Lagrange multiplier technique and the penalty method as limiting cases and alleviates some of their drawbacks. Although the perturbed Lagrangian formulation can be interpreted as a mixed method, it has been used only in conjunction with displacement finite element models (see Simo, Wriggers, and Taylor 1985; Stein, Wagner, and Wriggers 1986; and Wriggers, Wagner, and Stein 1987). Mixed formulations (with the fundamental unknowns consisting of the generalized displacements and internal forces) were shown to be considerably simpler for the treatment of highly nonlinear problems than displacement formulations. Therefore, the question arises as to whether the use of the perturbed Lagrangian formulation in conjunction with mixed finite element models might result in a more effective computational strategy for contact problems. The present study focuses on this question. Specifically, the objectives of this paper are (1) to present simple mixed finite element models and a computational procedure based on the perturbed Lagrangian formulation for the solution of contact problems and (2) to demonstrate the effectiveness of the models and the proposed procedure by means of numerical examples.

To sharpen the focus of the study, only frictionless contact of axisymmetric shells and curved beams is considered. The effects of large rotations and transverse shear deformation are accounted for, and the material of the structures is assumed to be linearly elastic and isotropic.

Notation

A	cross-sectional area of the beam
E	Young's modulus of the material
$[F]$	flexibility matrix for an individual element
G	shear modulus of the material
$\{G(X)\}$, $\{M(H,X)\}$	vectors of nonlinear terms in the element equations
$\tilde{f}(Z,p)$	vector defined in equations (6)
$\{\tilde{G}(Z)\}$	vector of nonlinear contributions to the global equations
$\overline{g}$	current gap (measured in the direction of the normal to the contact surface)
$\overline{g}_o$	initial gap
$\{g_o\}$	vector of initial gaps for the contact element
$\{H\}$	vector of internal force parameters
h	shell thickness
I	moment of inertia of the beam cross section
$[\tilde{K}]$	global linear matrix of the structure
M_n	moment resultant turning about the normal to the middle surface of the shell (see fig. 1)
M_s, M_θ	meridional and circumferential (hoop) bending stress resultants (see fig. 1)
N	shape functions used for approximating the generalized displacements and the Lagrange multipliers

N_s, N_θ	meridional and circumferential (hoop) stress resultants (see fig. 1)
P	concentrated load on beam (or ring load on shell)
$\{P\}$	normalized external load vector
$\{\tilde{P}\}$	global vector of normalized external loads and initial gaps
P_n	nodal force normal to the contact surface
p	load parameter
p_o	intensity of pressure load (internal pressures have positive sign)
$[Q], [R]$	elemental matrices associated with the contact condition and the regularization term in the functional
Q_s	transverse shear stress resultant (see fig. 1)
r	radius of hemispherical shell (see fig. 1)
r_o	radius of curvature of circular ring and hemispherical shell
$[S]$	strain-displacement matrix for an individual element
s	tangential coordinate along the undeformed centerline of the beam or meridional coordinate of the undeformed shell (see fig. 1)
s_i, s_e	values of s at the initial and the last point of the contact region
T_n	intensity of contact pressure (acting normal to the contact surface)
U	strain energy of the structure
$\overline{U}$	strain energy density (strain energy per unit length for beam or per unit area for shell)
u, w	displacement components in the x_1 and x_3 coordinate directions (see fig. 1)
$\{X\}$	vector of nodal displacements
x_1, x_2, x_3	Cartesian coordinates (for a shell x_3 coincides with the axis of revolution; see fig. 1)
$\{Z\}$	global response vector
$\alpha_H, \alpha_X, \alpha_\lambda, \alpha, \beta$	preselected constants used in the constraint equation (see eqs. (7) and (8))
γ_o	transverse shear strain
ε	penalty parameter
ε_s, γ_s	virtual extensional and transverse shear strains
ε_{so}	extensional strain (in the meridional direction of the shell or along the length of a beam)
ε_θ	extensional strain in the circumferential direction for a shell
ζ	generalized arc-length parameter defined in equations (7) and (8)
κ_n	bending strain associated with the moment turning about the normal to the shell M_n
κ_s	bending strain for a beam (or meridional bending strain for a shell)
κ_θ	circumferential (hoop) bending strain for a shell
$\overline{\lambda}$	Lagrange multiplier, representing the intensity of the contact pressure (acting normal to the contact surface)
$\{\lambda\}$	vector of nodal values of the Lagrange multiplier
ν	Poisson's ratio of the material
Π	functional
ϕ	rotation component of the beam or the middle surface of the shell
$\overline{\phi}$	$= \phi + \phi_0$
ϕ_0	angle which a typical cross section of the undeformed beam makes with the x_3-axis (or angle between the axis of revolution and the normal to the shell middle surface, see fig. 1)
$\Omega^{(e)}$	element domain
Ω_c	contact surface
∂_s	$\equiv d/ds$

Subscripts:

a	at point a of circular ring in figure 11

b	at point b of hemispherical shell in figure 3
conv.	converged

Superscript t denotes transposition.

Finite elements are designated M3-2 and M4-3 as shown in table 1.

Mathematical Formulation

The analytical formulation is based on a form of Reissner's large-rotation theory with the effects of transverse shear deformation included. A mixed formulation is used in which the fundamental unknowns consist of the three generalized displacements and the internal forces (five for shells of revolution and three for curved beams). The sign convention for the generalized displacements and the internal forces is given in figure 1. The fundamental equations of the axisymmetric shell theory and the curved beam theory used herein are given by Reissner (1972a, 1972b) and are summarized in appendix A.

Contact Condition

Figure 2 shows the characteristics of the frictionless contact of a structure pressed against a rigid plate: Ω_c refers to the contact region; $\overline{g}_o$ is the initial gap between the structure and the plate; $\overline{g}$ is the current gap (both $\overline{g}_o$ and $\overline{g}$ are measured in the direction of the normal to Ω_c); and T_n is the normal traction on Ω_c. The contact condition can be expressed by the following inequalities, which must be satisfied at each point on the contact surface Ω_c:

$$\overline{g} \geq 0 \qquad T_n \leq 0 \qquad T_n \overline{g} = 0 \tag{1}$$

The first inequality in equations (1) represents the kinematic condition of no penetration of the rigid plate (zero gap for the contact points); the second inequality is the static condition of compressive (or zero) normal tractions; and the third condition is that of zero work done by the contact stresses (i.e., the contact stresses exist only at the points where the structure is in contact with the rigid plate). The inequalities $\overline{g} > 0$ and $T_n > 0$ are henceforth referred to as the "inactive contact conditions."

Governing Finite Element Equations

The discrete equations governing the response of the structure are obtained by applying a modified form of the two-field Hellinger-Reissner mixed variational principle. The modification consists of augmenting the functional of that principle by two terms: the Lagrange multiplier associated with the nodal contact pressures and a regularization term which is quadratic in the Lagrange multipliers. For a detailed discussion of the perturbed and augmented Lagrangian formulations, see Simo, Wriggers, and Taylor (1985); Stein, Wagner, and Wriggers (1986); and Wriggers, Wagner, and Stein (1987).

The modified functional has the following form:

$$\Pi = \Pi_{HR} + \int_{\Omega_c} \left[\overline{\lambda} \overline{g} - \frac{1}{2\varepsilon} \left(\overline{\lambda} \right)^2 \right] d\Omega \tag{2}$$

where Π_{HR} is the functional of the Hellinger-Reissner variational principle; $\overline{\lambda}$ is the Lagrange multiplier; and ε is a penalty parameter associated with the regularization term. The explicit form of Π_{HR} for planar deformation of curved beams is given by Noor, Peters, and Andersen (1984); and for axisymmetric deformation of shells of revolution, by Noor, Andersen, and Tanner (1984). Note that the addition of the regularization term amounts to approximating the rigid plate by continuously distributed springs with stiffness of ε, for sufficiently large ε. As ε approaches zero, the continuous springs become the rigid plate.

The shape functions used in approximating the generalized displacements and the Lagrange multipliers are selected to be the same and differ from those used in approximating the internal forces. Moreover, because of the nature of the functional Π in equation (2), the continuity of both the internal forces and the Lagrange multipliers is not imposed at interelement boundaries.

The finite element equations for each individual element can be cast in the following compact form:

$$\begin{bmatrix} -F & S & \cdot \\ S^t & \cdot & Q \\ \cdot & Q^t & \frac{R}{\varepsilon} \end{bmatrix}^{(e)} \begin{Bmatrix} H \\ X \\ \lambda \end{Bmatrix}^{(e)} + \begin{Bmatrix} G(X) \\ M(H,X) \\ \cdot \end{Bmatrix}^{(e)} - \begin{Bmatrix} \cdot \\ pP \\ g_o \end{Bmatrix}^{(e)} = 0 \tag{3}$$

where $\{H\}, \{X\}$, and $\{\lambda\}$ are the vectors of the internal force parameters, nodal values of the generalized displacements, and nodal values of the Lagrange multipliers; $[F]$ is the matrix of linear flexibility coefficients; $[S]$ is the strain-displacement matrix; $[Q]$ and $[R]$ are matrices associated with the contact condition and the regularization term in the functional (see appendix B); $\{G(X)\}$ and $\{M(H,X)\}$ are vectors of nonlinear terms; $\{g_o\}$ is the vector of initial gaps in the contact region; a dot refers to a zero submatrix or a zero subvector; superscript (e) refers

to individual elements; $\{P\}$ is the normalized external load vector; and p is a load parameter. As the load is incremented, only the value of the load parameter p changes and the normalized vector $\{P\}$ is constant. The formulas for the elemental arrays $[F], [S], \{G(X)\}, \{M(H,X)\}$, and $\{P\}$ are given by Noor, Peters, and Andersen (1984) for curved beams and by Noor, Andersen, and Tanner (1984) for axisymmetric shells. The formulas for the elemental arrays $[Q]$ and $[R]$ are given in appendix B.

Note that the size of the coefficient matrices $[R]$, $[Q]$, and $\{g_o\}$ varies with the number of active contact conditions. The difficulty associated with an equation system whose size varies during the solution process can be alleviated by allowing the Lagrange multipliers to be discontinuous at interelement boundaries and eliminating them on the element level. This was done in the present study. If the internal force parameters and the Lagrange multiplier parameters are eliminated from equations (3), one obtains the following equations in the nodal displacements $\{X\}$:

$$\left[[S]^t[F]^{-1}[S] - \varepsilon[Q][R]^{-1}[Q]^t\right]^{(e)}\{X\}^{(e)} + \{\overline{G}(X)\}^{(e)} + \varepsilon[Q][R]^{-1}\{g_o\}^{(e)} - p\{P\}^{(e)} = 0 \tag{4}$$

where

$$\{\overline{G}(X)\}^{(e)} = [S]^t[F]^{-1}\{G(X)\}^{(e)} + \{M(H,X)\} \tag{5}$$

and the vector $\{H\}$ in $\{M(H,X)\}$ is replaced by its expression in terms of $\{X\}$.

Solution of Nonlinear Algebraic Equations

The discrete equations governing the response of the entire structure are obtained by assembling the elemental contributions in equations (3) or (4) and can be written in the following compact form:

$$\{\tilde{f}(Z,p)\} = [\tilde{K}]\{Z\} + \{\tilde{G}(Z)\} - p\{\tilde{P}\} = 0 \tag{6}$$

where $[\tilde{K}]$ is the global linear matrix of the structure; $\{\tilde{G}(Z)\}$ is the vector of nonlinear contributions; $\{\tilde{P}\}$ is the global vector of normalized external loads and initial gaps; and $\{Z\}$ is the global response vector of the structure (obtained by assembling the contributions from the subvectors $\{H\}, \{X\}$, and $\{\lambda\}$).

The nonlinear algebraic equations (eqs. (6)) are solved and the contact region and the contact pressures are determined by using an incremental-iterative technique (i.e., a predictor-corrector continuation method) in which the response vector $\{Z\}$, corresponding to a particular value of the load parameter p, is used to calculate a suitable approximation (predictor) for $\{Z\}$ at a different value of p. This approximation is then chosen as an initial estimate for $\{Z\}$ in a corrective iterative scheme such as the Newton-Raphson technique. In each Newton-Raphson iteration the contact conditions are checked and updated.

Generalized Arc Length and Associated Constraint Equation

A number of numerical experiments have demonstrated that a more effective computational algorithm results if $\{X\}, \{H\}, \{\lambda\}$, and p are considered functions of a nondecreasing parameter ζ which is defined by the following constraint equations (see, for example, Ramm 1981):

$$\alpha_H\left\{\frac{\partial H}{\partial \zeta}\right\}^t\left\{\frac{\partial H}{\partial \zeta}\right\} + \alpha_X\left\{\frac{\partial X}{\partial \zeta}\right\}^t\left\{\frac{\partial X}{\partial \zeta}\right\} + \alpha_\lambda\left\{\frac{\partial \lambda}{\partial \zeta}\right\}^t\left\{\frac{\partial \lambda}{\partial \zeta}\right\} + \beta\left(\frac{\partial p}{\partial \zeta}\right)^2 = 1 \tag{7}$$

where α_H, α_X, α_λ, and β are preselected constants ($0 \le \alpha_H, \alpha_X, \alpha_\lambda, \beta \le 1$), and superscript t denotes transposition. If $\alpha_H = \alpha_X = \alpha_\lambda = \beta = 1$, then ζ represents the arc length in the space spanned by $\{H\}, \{X\}, \{\lambda\}$, and p. Therefore, ζ in equations (7) represents a generalized arc length in the solution space.

In the present study α_H, α_X, and α_λ were all taken to be equal, that is, $\alpha_H = \alpha_X = \alpha_\lambda = \alpha$, so that equations (7) can be written in the form:

$$\alpha\left\{\frac{\partial Z}{\partial \zeta}\right\}^t\left\{\frac{\partial Z}{\partial \zeta}\right\} + \beta\left(\frac{\partial p}{\partial \zeta}\right)^2 = 1 \tag{8}$$

To retain the symmetry and bandedness of the resulting finite element equations of the structure, the constraint equations (eqs. (7) or (8)) are not solved simultaneously with equations (6); rather, the two-step procedure outlined by Ramm (1981) is used (see appendix C). The use of ζ as the parameter controlling the progress of computation along the solution path, in addition to circumventing the problems associated with the singularity of the system matrix at limit points, has other computational advantages that are discussed in the section on numerical studies.

Computational Procedure and Determination of Contact Pressures

The computational procedure used in determining the contact region and the contact pressures is outlined in appendix C. The nonlinearities due to the large rotations and the contact condition are combined into a single iteration loop. Wriggers and Nour-Omid (1984) advocated the use of a two-level (nested) iteration scheme. The inner iteration loop accounts for the contact conditions associated with the contact pressures, and the outer iteration loop uses Newton-Raphson iteration. Numerical experiments have demonstrated that for frictionless contact problems the two-level iterative scheme requires more iterations than the single-level scheme. This is discussed further in the section on numerical studies.

The solution of the governing discrete equations of the entire structure generates the nodal displacements, the internal force parameters, and the values of the Lagrange multipliers at the contact nodes. For each individual element in contact, the intensity of the contact pressure at a node T_n is equal to the value of the Lagrange multiplier λ at the same node. The contact pressures are also related to the nodal forces normal to the contact P_n^i as follows:

$$P_n^i = \int_{\Omega^{(e)}} N^i N^j \, d\Omega \, T_n^j \tag{9}$$

where N^i are the shape functions used in approximating the Lagrange multiplier and the generalized displacements and $\Omega^{(e)}$ is the domain of the contact element. The range of both i and j in equations (9) is from 1 to the number of displacement nodes. Torstenfelt (1983) discusses other approaches for determining the contact pressures.

Comments on the Mixed Models, Perturbed Lagrangian Formulation, and Computational Procedure

The following comments regarding the mixed models, the perturbed Lagrangian formulation and the computational procedure used herein are in order:

1. The nonlinear terms in the finite element equations of the mixed model (eqs. (3)) have a considerably simpler form than those of the corresponding displacement model (eqs. (5)). This is particularly true for large rotation problems (for a more detailed comparison between mixed and displacement finite element models, see Noor, Peters, and Andersen 1984; and Noor, Andersen, and Tanner 1984).
2. Equations (3) include both those of the Lagrange multiplier approach and the penalty method as special cases, as follows:
   a. By letting the penalty parameter ε go to infinity, equations (3) reduce to those of the Lagrange multiplier approach.
   b. By eliminating the Lagrange multiplier terms from equations (3), the resulting equations are identical to those of the penalty method.
3. The perturbed Lagrangian formulation alleviates two of the drawbacks of the Lagrange multiplier approach and the penalty method, namely,
   a. The regularization term in the functional results in replacing one of the zero diagonal blocks in the discrete equations of the Lagrange multiplier approach by the diagonal matrix $[R]/\varepsilon$ in equations (3).
   b. The contact condition is satisfied exactly by transforming the constrained problem to an unconstrained one through the introduction of Lagrange multipliers (the term $\int_{\Omega_c} \bar{\lambda}\bar{g} \, d\Omega$ in eq. (2)) rather than approximately as in the penalty method. However, the presence of the regularization term (the term $-\int_{\Omega_c}(1/2\varepsilon)(\bar{\lambda})^2 \, d\Omega$ in eq. (2)) results in replacing the contact condition by the perturbed condition,

$$\frac{1}{\varepsilon}[R]\{\lambda\} + [Q]^t\{X\} - \{g_o\} = 0 \tag{10}$$

4. An important consideration in the perturbed Lagrangian formulation (and in any penalty formulation) is the proper selection of the penalty parameter ε. With the foregoing mixed models the penalty parameter can be chosen independently of the element size, without adversely affecting the performance of the model. The accuracy of the solution increases with increasing value of the penalty parameter. However, for very large values of ε, the equations become ill-conditioned and thus round-off errors increase (see Felippa 1978). In the present study the penalty parameter ε was related to the extensional stiffness of the structure.
5. The elemental arrays $[F]$, $[S]$, $\{G(X)\}$, $\{M(H,X)\}$, and $\{P\}$ are evaluated numerically using a Gauss-Legendre formula. The arrays $[Q]$, $[R]$, and $\{g_o\}$ are evaluated using a Newton-Cotes formula. In both cases the number of quadrature points used is the same as the number of displacement nodes in the element. This results in underintegrating the arrays $[Q]$ and $[R]$ and avoids the oscillatory behavior of the contact pressures that has been

observed when these arrays are fully integrated. Note that the use of Newton-Cotes formula allows the contact pressures to be evaluated at the displacement nodes.

Numerical Studies

To test and evaluate the performance of the mixed models and the foregoing computational procedure, several frictionless contact problems have been solved by using this procedure. For each problem, comparison was made with converged solutions and with previously published numerical and analytic solutions (whenever available). Herein the results of two typical frictionless contact problems are discussed. The two problems are (1) a hemispherical shell in contact with a rigid plate (fig. 3) and (2) a circular ring pressed against a rigid plate (fig. 11). Updike and Kalnins (1972) give an analytic solution for the first problem. Finite element solutions using displacement models are presented by Stein, Wagner, and Wriggers (1986) for the hemispherical shell and by Simo et al. (1984) for the circular ring. In the cited references only load-deflection curves and distribution of contact stresses were presented. The material for both structures is assumed to be linearly elastic and isotropic, and the effects of both large rotations and transverse shear deformation are accounted for (see appendix A). For the hemispherical shell, only axisymmetric deformations are considered and therefore, only one meridian was modeled. For the circular ring only planar deformation is considered, and because of symmetry, only half the ring was modeled.

In each case the structure was analyzed using the mixed models developed herein. Lagrangian interpolation functions were used for approximating each of the generalized displacements, internal forces, and Lagrange multipliers. For convenience, the values of α and β in the generalized arc-length constraint equations (eqs. (6) and (7)) were selected to be unity. The characteristics of the mixed finite element models used herein are summarized in table 1. No convergence or other difficulties were encountered in applying the foregoing computational procedure to the two problems. The converged solutions obtained by the mixed models were found to be in close agreement with the analytic solutions of Updike and Kalnins (1972) and the finite element solutions of Stein, Wagner, and Wriggers (1986) and Simo et al. (1984). Typical results are presented in figures 4 through 10 for the hemispherical shell and in figures 12 through 15 for the circular ring. The results presented in figures 4 through 15 are considerably more extensive than previously reported and are intended to give physical insight into the response of the two structures. All the numerical studies were performed on the Control Data Corp. CYBER 180-860 computer at NASA Langley Research Center.

Hemispherical Shell in Contact With a Rigid Plate

The first problem considered is the hemispherical shell pressed against a rigid flat plate. The geometric and material characteristics of the shell are shown in figure 3. Two cases are considered. In the first case the shell is subjected to a uniform ring load P and in the second case the shell is subjected to uniform internal pressure p_o in addition to the ring load. The first case is similar to that presented by Stein, Wagner, and Wriggers (1986) and Updike and Kalnins (1972). However, even in this case the results presented herein are for a much higher loading range than that considered in the cited references.

The shell was modeled using uniform and nonuniform grids of the M3-2 and M4-3 elements (see table 1), with small-size elements in the contact zone. The converged solutions presented herein correspond to a nonuniform grid of 30 M3-2 elements. The characteristics of the nonuniform grids used are summarized in table 2. The variations in the vertical displacement at the loaded end and in the strain energy components with the ring loading are shown in figure 4. The deformed configurations of the shell for different combinations of P and p_o are shown in figure 5. The distribution of the strain energy densities and the contact pressures along the meridian, for different values of p_o and P, are shown in figures 6 and 7. As can be seen from figure 6, both the bending and the transverse shear strain energy has a localized character. The variation of the contact region with loading is shown in figure 8. In the absence of internal pressure a gap develops between the shell and the plate, with increasing loading. However, the size of the gap is too small to be noticeable (see fig. 5), and, as expected, the presence of internal pressure reduces the gap and increases the contact area. For $p_o/E = 5 \times 10^{-5}$, no gap develops throughout the range of the ring loading considered. The predictions of the M3-2 and M4-3 models are shown in figure 9. For the same number of degrees of freedom, the two models result in comparable accuracy. This may be attributed to the fact that the accuracy is governed by the contact conditions.

The number of iterations required for both the load and the arc-length incrementation is given in table 3. The number of iterations required for the two-level iteration scheme proposed by Wriggers and Nour-Omid (1984) is also given in table 3. As can be seen from table 3, use of the arc-length incrementation in conjunction with the single-level

iteration scheme is more efficient than the other schemes.

The effect of the magnitude of the penalty parameter on the accuracy of the total strain energy obtained by the mixed models, at $Pr_o/Eh^2 = 2.0$ and $p_o = 0$, is depicted in figure 10. As can be seen, the accuracy of the total strain energy obtained by the mixed models is fairly insensitive to the choice of ε in the range of ε/Eh from 10^3 to 10^{10}.

Circular Ring Pressed Against a Rigid Plate

The second problem is a circular ring pressed against a rigid plate by a concentrated load at the top. The geometric and material characteristics of the ring are shown in figure 11. The ring was modeled by using uniform grids of M3-2 and M4-3 elements.

The deformation of the ring is nearly inextensional, with both the extensional and the transverse shear strain energy equal to zero throughout the range of loading considered. The total strain energy is essentially equal to the bending energy. The accuracy of the vertical displacement w_a and the strain energies U obtained by using the M3-2 and M4-3 models is depicted in figure 12. Again, both models gave comparable accuracy. The deformed configurations of the ring are shown in figure 13 along with the distribution of the total strain energy density along the meridian, for different values of the concentrated load.

The variation of the contact region with loading is depicted in figure 14. As can be seen from figure 14, only a small segment of the ring remains in contact, for any given value of the load. However, the gap is very small and cannot be noticed in figure 13.

The effect of the magnitude of the penalty parameter on the accuracy of the total strain energy obtained by the mixed models, at $Pr_o^2/EI = 2.863$, is depicted in figure 15. Again the accuracy of the total strain energy is fairly insensitive to the choice of ε in the range of ε/EA from 10^{-5} to 10^4.

Concluding Remarks

Simple mixed finite element models and a computational procedure are presented for the solution of frictionless contact problems. The analytical formulation is based on a form of Reissner's large-rotation theory of the structure with the effect of transverse shear deformation included. The contact conditions are incorporated into the formulation by using a perturbed Lagrangian approach with the fundamental unknowns consisting of the internal forces (or stress resultants), the generalized displacements, and the Lagrange multipliers associated with the contact conditions. The elemental arrays are obtained by using a modified two-field mixed variational principle. The modification consists of augmenting the functional of that principle by two terms: the Lagrange multiplier vector associated with the nodal contact pressures and a regularization term which is quadratic in the Lagrange multiplier vector.

The shape functions used in approximating the generalized displacements and the Lagrange multipliers are selected to be the same and are different from those used in approximating the internal forces. The internal forces and the Lagrange multipliers are allowed to be discontinuous at interelement boundaries. The nonlinearities due to both the large rotations and the contact conditions are combined into the same iteration loop and are handled by using the Newton-Raphson iterative scheme.

Two numerical examples of axisymmetric deformations of a hemispherical shell and planar deformations of a circular ring are presented. Both structures are pressed against a rigid plate. The detailed information presented herein is considerably more extensive than previously reported and helps in gaining physical insight about the response of both structures. The numerical studies have demonstrated the high accuracy of the mixed models and the effectiveness of the computational procedure, which combines both the geometrically nonlinear terms and the contact conditions in one iteration loop.

NASA Langley Research Center
Hampton, VA 23665-5225
February 6, 1989

Appendix A

Fundamental Equations of the Large-Rotation Theories Used in the Present Study

The fundamental equations of the large-rotation theories of Reissner (1972a, 1972b) for shells of revolution and curved beams are summarized herein. For shells of revolution, only axisymmetric deformations are considered, and the effects of transverse shear deformation and moments turning around the normal to the middle surface are included. For curved beams, only planar deformation is considered, and the effects of transverse shear deformation and centerline extensibility are included. A total Lagrangian description of the deformation is used, and the structure configurations at different load levels are referred to the initial coordinate system of the undeformed structure.

Strain-Displacement Relationships

The relationships between the strains and the generalized displacements are given as follows. For both the shell of revolution and the curved beam, the expressions for ε_s, κ_s, and γ_s are

$$\begin{aligned}\varepsilon_s &= \cos(\phi+\phi_o)\,\partial_s u - \sin(\phi+\phi_o)\,\partial_s w + \cos\phi - 1\\ &= (1+\varepsilon_{so})\cos\gamma_o - 1\\ \kappa_s &= \partial_s \phi\\ \gamma_s &= \sin(\phi+\phi_o)\,\partial_s u + \cos(\phi+\phi_o)\,\partial_s w + \sin\phi\\ &= (1+\varepsilon_{so})\sin\gamma_o\end{aligned}$$

In addition, for the shell of revolution, the expressions for ε_θ, κ_θ, and κ_n are

$$\begin{aligned}\varepsilon_\theta &= \frac{u}{r}\\ \kappa_\theta &= \frac{1}{r}\left[\sin(\phi+\phi_o) - \sin\phi_o\right]\\ \kappa_n &= \frac{1}{r}\left[\cos(\phi+\phi_o) - \cos\phi_o\right]\end{aligned}$$

where ε_{so} is the extensional strain (relative change of length in the s-direction); γ_o is the transverse shearing strain; κ_s is the bending strain in the s-direction; ε_s and γ_s are virtual extensional and shearing strains; ε_θ and κ_θ are the extensional and bending strains in the circumferential directions for the shell; κ_n is the bending strain associated with the moment turning about the normal to the middle surface of the shell; and $\partial_s \equiv d/ds$.

Constitutive Relations

The material of the structures is assumed to be linearly elastic and isotropic. The relations between the strain components and the internal forces (stress resultants) are given in table A1. In table A1, E, G, and ν are Young's modulus, shear modulus, and Poisson's ratio of the material; h is the shell thickness; and A and I are the cross-sectional area and the moment of inertia of the curved beam.

Table A1. Constitutive Relations

	Shell of revolution	Curved beam
Extensional group	$\begin{Bmatrix}\varepsilon_s\\ \varepsilon_\theta\end{Bmatrix} = \frac{1}{Eh}\begin{bmatrix}1 & -\nu\\ -\nu & 1\end{bmatrix}\begin{Bmatrix}N_s\\ N_\theta\end{Bmatrix}$	$\varepsilon_s = \frac{1}{EA}N_s$
Bending group	$\begin{Bmatrix}\kappa_s\\ \kappa_\theta\\ \kappa_n\end{Bmatrix} = \frac{12}{Eh^3}\begin{bmatrix}1 & -\nu & \cdot\\ -\nu & 1 & \cdot\\ \cdot & \cdot & 1-\nu^2\end{bmatrix}\begin{Bmatrix}M_s\\ M_\theta\\ M_n\end{Bmatrix}$	$\kappa_s = \frac{1}{EI}M_s$
Transverse shear	$\gamma_s = \frac{1}{Gh}Q_s$	$\gamma_s = \frac{1}{GA}Q_s$

Appendix B

Formulas for the Elemental Arrays $[Q]$, $[R]$, and $\{g_o\}$

The explicit forms of the elemental arrays $[Q]$, $[R]$, and $\{g_o\}$ are given in this appendix. For convenience, each array is partitioned into blocks according to contributions from displacement and contact nodes. The expressions of the typical partitions (or blocks) are given in table B1. In table B1, N^i and N^j are the shape functions for the Lagrange multipliers and generalized displacements; m is the number of displacement nodes in the element; c is the number of nodal points in contact in the element; and $\Omega^{(e)}$ is the element domain. The range of the indices i and j is from 1 to c, and the range of the index i' is from 1 to m; and $< \tilde{g} >$ is the unit ramp (or singularity) function defined as follows:

$$< \tilde{g} >^n = \begin{cases} \tilde{g}^n & (\tilde{g} > 0) \\ 0 & (\tilde{g} \leq 0) \end{cases}$$

where $\tilde{g} = -\bar{g}$ and n = 0 or 1.

Table B1. Explicit Form of Typical Partitions of Arrays $[Q]$, $[R]$, and $\{g_o\}$

Array	Number of partitions or blocks	Formula for typical partition
$[Q]$	$m \times c$	$\int_{\Omega^{(e)}} N^{i'} N^j < \tilde{g} >^0 \, d\Omega$
$[R]$	$c \times c$	$-\int_{\Omega^{(e)}} N^i N^j < \tilde{g} >^0 \, d\Omega$
$\{g_o\}$	c	$\int_{\Omega^{(e)}} N^i < \tilde{g}_o > \, d\Omega$

Appendix C

Computational Procedure Based on Generalized Arc-Length Control

The computational procedure (see Ramm 1981) used in the present study is summarized in this appendix.

Preprocessing and Initial Calculation Phase

- Step 1. Input problem and model data; select values for the parameters α and β; select estimates for the penalty parameter and the generalized arc-length increment $\Delta\zeta$ (see Noor and Peters 1981a, 1981b); and assume the contact status at the different nodes.
- Step 2. Generate linear elemental arrays.

Solution Phase

- Begin incrementation loop.
- Begin Newton-Raphson iteration loop.
  - Step 3. Predict the generalized displacements, internal forces (stress resultants), and Lagrange multipliers for the structure.
  - Step 4. Generate the vector $\{\partial Z/\partial\zeta\}_i$ using the following set of equations:

$$\left[[\tilde{K}] + \left[\frac{\partial \tilde{G}_I}{\partial Z_J}\right]\right]\left\{\frac{\partial Z}{\partial p}\right\}_i = \{\tilde{P}\}$$

$$\left.\frac{\partial p}{\partial \zeta}\right|_i = \pm\left[\beta + \alpha\left\{\frac{\partial Z}{\partial p}\right\}_i^t\left\{\frac{\partial Z}{\partial p}\right\}_i\right]^{-1/2}$$

$$\left\{\frac{\partial Z}{\partial \zeta}\right\}_i = \left\{\frac{\partial Z}{\partial p}\right\}_i \left.\frac{\partial p}{\partial \zeta}\right|_i$$

  where the range of I and J is from 1 to the number of degrees of freedom in the model; and subscript i refers to the ith incrementation step. The positive sign for $\partial p/\partial\zeta$ is taken for the stable equilibrium path and the negative sign for the unstable path (see Noor and Peters 1981a, 1981b).

  - Step 5. Complete initial estimates for $(\Delta p)_i$ and $\{\Delta Z\}_i$ as follows:

$$(\Delta p)_i^{(1)} = \left.\frac{\partial p}{\partial \zeta}\right|_i \Delta\zeta$$

$$\{\Delta Z^{(1)}\}_i = \left\{\frac{\partial Z}{\partial \zeta}\right\}_i \Delta\zeta$$

  - Step 6. Generate nonlinear elemental array; eliminate the internal forces and the Lagrange multipliers from the elemental equations; and assemble the left- and right-hand sides of the equations.
  - Step 7. The change $\{\Delta Z\}$ in the response vector $\{Z\}$ during the ith incrementation step can be expressed as the sum of the two vectors

$$\{\Delta Z\}_i = \{\Delta\overline{Z}\}_i + (\Delta p)_i\{\Delta\widehat{Z}\}_i$$

  The vectors $\{\Delta\overline{Z}\}$ and $\{\Delta\widehat{Z}\}$ are obtained by solving the following system of algebraic equations:

$$\left[[\tilde{K}] + \left[\frac{\partial \tilde{G}_I^{(r)}}{\partial Z_J}\right]\right]\left[\left\{\Delta\overline{Z}^{(r)}\right\}\left\{\Delta\widehat{Z}^{(r)}\right\}\right] = \left[-\left\{\tilde{f}(Z,p)^{(r)}\right\}\left\{\tilde{P}\right\}\right]$$

where superscript r refers to the rth iteration cycle, and subscript i has been dropped for convenience.

- Step 8. Calculate the incremental load factor Δp using the equation

$$\Delta p^{(r)} = \frac{-\alpha \left\{\Delta Z^{(1)}\right\}^t \left\{\Delta \overline{Z}^{(r)}\right\}}{\alpha \left\{\Delta Z^{(1)}\right\}^t \left\{\Delta \widehat{Z}^{(r)}\right\} + \beta \Delta p^{(1)}}$$

- Step 9. Update the load factor and the response vector

$$p^{(r+1)} = p^{(r)} + \Delta p^{(r)}$$

$$\left\{Z^{(r+1)}\right\} = \left\{Z^{(r)}\right\} + \left\{\Delta Z^{(r)}\right\}$$

- Step 10. Check the contact status (and modify the contact conditions) at each node as needed: If $\overline{g} > 0$ and $\lambda > 0$, then the constraint is inactive; if $\overline{g} \leq 0$, then the constraint is active. If contact status is the same as previously assumed, then continue. Otherwise, add the contact contributions for nodes with active constraint and delete these contributions for nodes with inactive constraint; then return to step 6.

- Step 11. Check convergence of Newton-Raphson iterations, that is,

$$e = \frac{\left[\{\Delta Z\}^t \{\Delta Z\} / \{Z\}^t \{Z\}\right]^{1/2}}{n} \leq \text{Tolerance}$$

where n is the total number of degrees of freedom in the model; and the tolerance is prescribed. If convergence is achieved then continue; otherwise return to step 6.

- Step 12. If $p \geq p_{\max}$, then stop; otherwise set $\zeta = \zeta + \Delta\zeta$ and return to step 3.

References

Felippa, Carlos A. 1978: Iterative Procedures for Improving Penalty Function Solutions of Algebraic Systems. *Int. J. Numer. Methods Eng.*, vol. 12, no. 5, pp. 821–836.

Kalker, J. J. 1986: The Principle of Virtual Work and Its Dual for Contact Problems. *Ing. Archiv*, vol. 56, no. 6, pp. 453–467.

Kikuchi, N.; and Oden, J. T. 1988: *Contact Problems in Elasticity: A Study of Variational Inequalities and Finite Element Methods.* SIAM.

Kikuchi, Noboru; and Song, Young Joon 1981: Penalty/Finite-Element Approximations of a Class of Unilateral Problems in Linear Elasticity. *Q. Appl. Math.*, vol. 39, no. 1, Apr. pp. 1–22.

Noor, Ahmed K.; Andersen, Carl M.; and Tanner, John A. 1984: *Mixed Models and Reduction Techniques for Large-Rotation, Nonlinear Analysis of Shells of Revolution With Application to Tires.* NASA TP-2343.

Noor, Ahmed K.; and Peters, Jeanne M. 1981a: Bifurcation and Post-Buckling Analysis of Laminated Composite Plates Via Reduced Basis Technique. *Comput. Methods Appl. Mech. & Eng.*, vol. 29, Dec., pp. 271–295.

Noor, Ahmed K.; and Peters, Jeanne M. 1981b: Tracing Post-Limit-Point Paths With Reduced Basis Technique. *Comput. Methods Appl. Mech. & Eng.*, vol. 28, no. 2, Sept., pp. 217–240.

Noor, Ahmed K.; Peters, Jeanne M.; and Andersen, Carl M. 1984: Mixed Models and Reduction Techniques for Large-Rotation Nonlinear Problems. *Comput. Methods Appl. Mech. & Eng.*, vol. 44, no. 1, June, pp. 67–89.

Noor, Ahmed K.; and Tanner, John A. 1988: *Advances in Contact Algorithms and Their Application to Tires.* NASA TP-2781.

Ramm, E. 1981: Strategies for Tracing the Nonlinear Response Near Limit Points. *Nonlinear Finite Element Analysis in Structural Mechanics*, W. Wunderlich, E. Stein, and K.-J. Bathe, eds., Springer-Verlag, pp. 63–89.

Reissner, Eric 1972a: On Finite Symmetrical Deflections of Thin Shells of Revolution. *Trans. ASME, Ser. E: J. Appl. Mech.*, vol. 36, no. 2, June, pp. 267–270; vol. 39, no. 4, Dec., pp. 1137–1138.

Reissner, Eric 1972b: On One-Dimensional Finite-Strain Beam Theory: The Plane Problem. *Z. Angew. Math. & Phys.*, vol. 23, Fasc. 5, Sept. 25, pp. 795–804.

Simo, J. C.; Wriggers, P.; Schweizerhof, K. H.; and Taylor, R. L. 1984: Finite Deformation Postbuckling Analysis Involving Inelasticity and Contact Constraints. *Innovative Methods for Nonlinear Problems*, W. K. Liu, T. Belytschko, and K. C. Park, eds., Pineridge Press International Limited (Swansea, U. K.), pp. 365–387.

Simo, Juan C.; Wriggers, Peter; and Taylor, Robert L. 1985: A Perturbed Lagrangian Formulation for the Finite Element Solution of Contact Problems. *Comput. Methods Appl. Mech. & Eng.*, vol. 50, no. 2, Aug., pp. 163–180.

Stadter, J. T.; and Weiss, R. O. 1979: Analysis of Contact Through Finite Element Gaps. *Comput. & Struct.*, vol. 10, no. 6, Dec., pp. 867–873.

Stein, E.; Wagner, W.; and Wriggers, P. 1986: Finite Element Postbuckling Analysis of Shells With Nonlinear Contact Constraints. *Finite Element Methods for Nonlinear Problems*, P. G. Bergan, K. J. Bathe, and W. Wunderlich, eds., Springer-Verlag, pp. 719–744.

Torstenfelt, Bo 1983: Finite Elements in Contact and Friction Applications. Linköping Studies in Science and Technology. Dissertations. No. 103, Div. of Solid Mechanics and Strength of Materials, Dep. of Mechanical Engineering, Linköping Univ. (Linköping, Sweden).

Updike, D. P.; and Kalnins, A. 1972: Contact Pressure Between an Elastic Spherical Shell and a Rigid Plate. *Trans. ASME, Ser. E: J. Appl. Mech.*, vol. 39, no. 4, Dec., pp. 1110–1114.

Wriggers, P.; Wagner, W.; and Stein, E. 1987: Algorithms for Non-Linear Contact Constraints With Application to Stability Problems of Rods and Shells. *Comput. Mech.*, vol. 2, pp. 215–230.

Wriggers, Peter; and Nour-Omid, Bahram 1984: *Solution Methods for Contact Problems.* Rep. No. UCB/SESM-84/09 (Contract N00014-76-C-0013), Dep. of Civil Engineering, Univ. of California, July.

Table 1. Characteristics of Mixed Finite Element Models Used in Numerical Studies

Designation	Number of displacement nodes	Maximum number of Lagrange multiplier nodes	Number of parameters per internal force	Number of quadrature points[a]
M3-2	3	3	2	3
M4-3	4	4	3	4

[a]All elemental arrays are evaluated using Gauss-Legendre quadrature formulas except for $[Q]$, $[R]$, and $\{g_o\}$ which are evaluated using Newton-Cotes formulas.

Table 2. Characteristics of Nonuniform Grids Used in Modeling Hemispherical Shell

$$\left[\text{Element length } l = r_o \pi \frac{\Delta\phi_o}{180}\right]$$

8 elements		12 elements		15 elements		30 elements	
Element no.	$\Delta\phi_o$, deg	Element no.	$\Delta\phi_o$, deg	Element no.	$\Delta\phi_o$, deg	Element no.	$\Delta\phi_o$, deg
1	1.5	1	1.0	1 to 10	3	1 to 20	1.5
2 to 4	9.5	2 to 6	5.8	11	5	21	2.0
5 to 8	15.0	7 to 12	10.0	12	9	22, 23	5.0
				13	13	24	6.0
				14	16	25 to 30	7.0
				15	17		

Table 3. Comparison of Number of Iterations Required for Present Single-Level Iteration Procedure With Two-Level Iteration Procedure

[Hemispherical shell in contact with a rigid plate (see fig. 3); 15 M3-2 elements along the meridian]

Step	Arc-length incrementation				Load incrementation		
	$\frac{Pr_o}{Eh^2}$	Single iteration loop[a]	$\frac{Pr_o}{Eh^2}$	Two iteration loops[b]	$\frac{Pr_o}{Eh^2}$	Single iteration loop[a]	Two iteration loops[b]
1	2.3442	5 (3)	2.3442	7	4.0	8 (5)	17
2	9.6426	5 (2)	9.6411	8	8.0	7 (6)	21
3	15.315	5 (10)	15.318	17	12.0	8 (5)	21
4	21.927	5 (5)	21.939	14	16.0	6 (3)	17
5	29.316	7 (5)	29.349	14	20.0	6 (7)	8
6	36.775	7 (4)	36.845	9	24.0	4 (7)	11
7	44.466	6 (4)	44.541	9	28.0	4 (3)	10
8	51.627	4 (8)	51.818	5	32.0	3 (8)	11
9					36.0	4 (3)	5
10					40.0	4 (5)	5
11					44.0	8 (8)	21
12					48.0	3 (3)	7
13					52.0	7 (3)	18
Total		44 (41)		83		72 (66)	172

[a]Numbers in parentheses indicate the number of iterations for the uniform grid; other numbers are for the nonuniform grid (see table 2). The prescribed tolerance was selected to be 1×10^{-5}.

[b]Based on the solution procedure of Wriggers and Nour-Omid (1984).

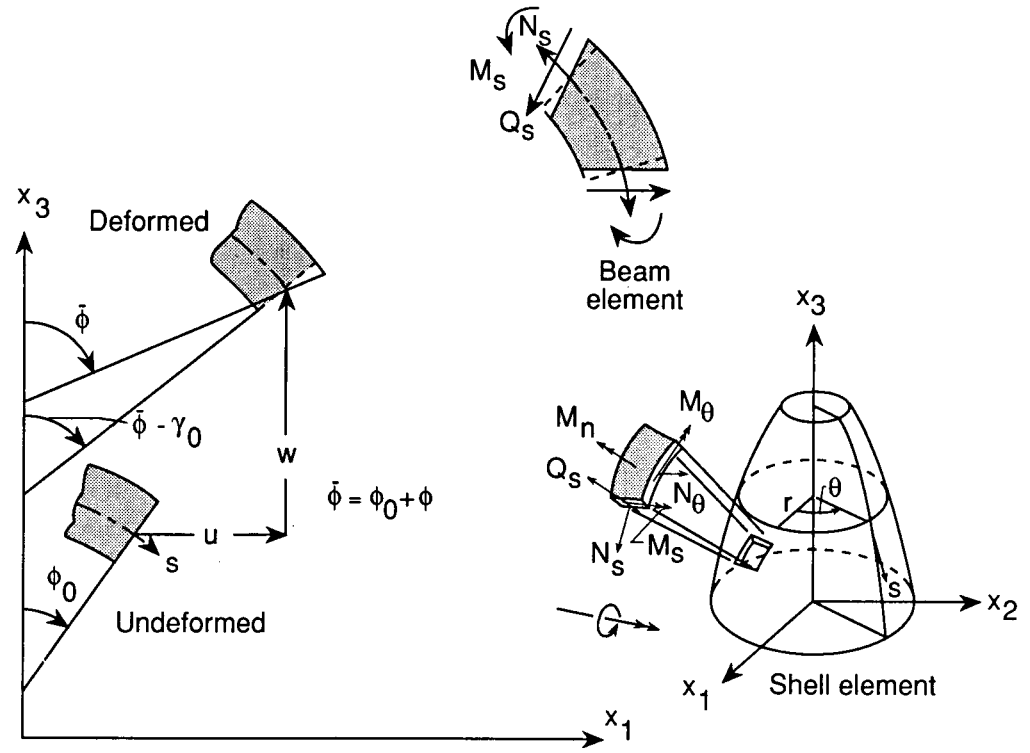

Figure 1. Curved beam and shell elements and sign convention.

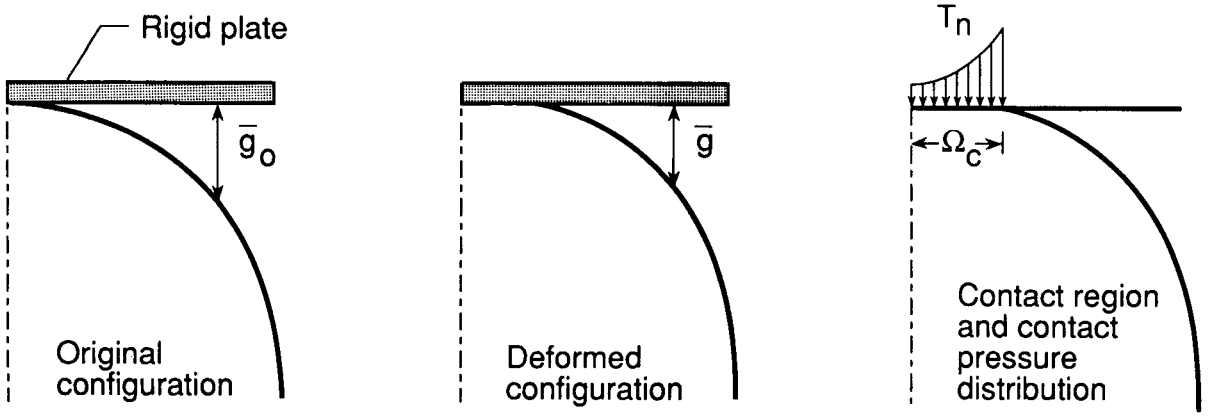

Figure 2. Characteristics of frictionless contact of a structure pressed against a rigid plate.

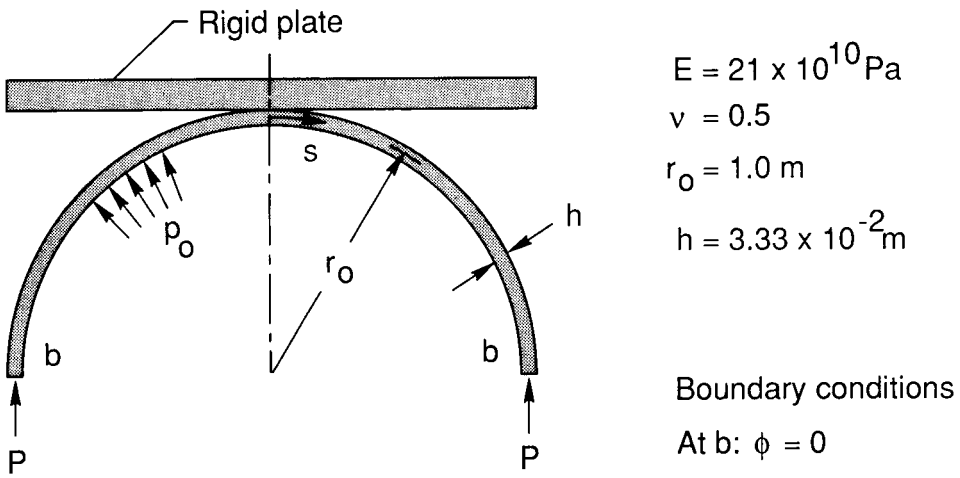

Figure 3. Hemispherical shell in contact with a rigid plate.

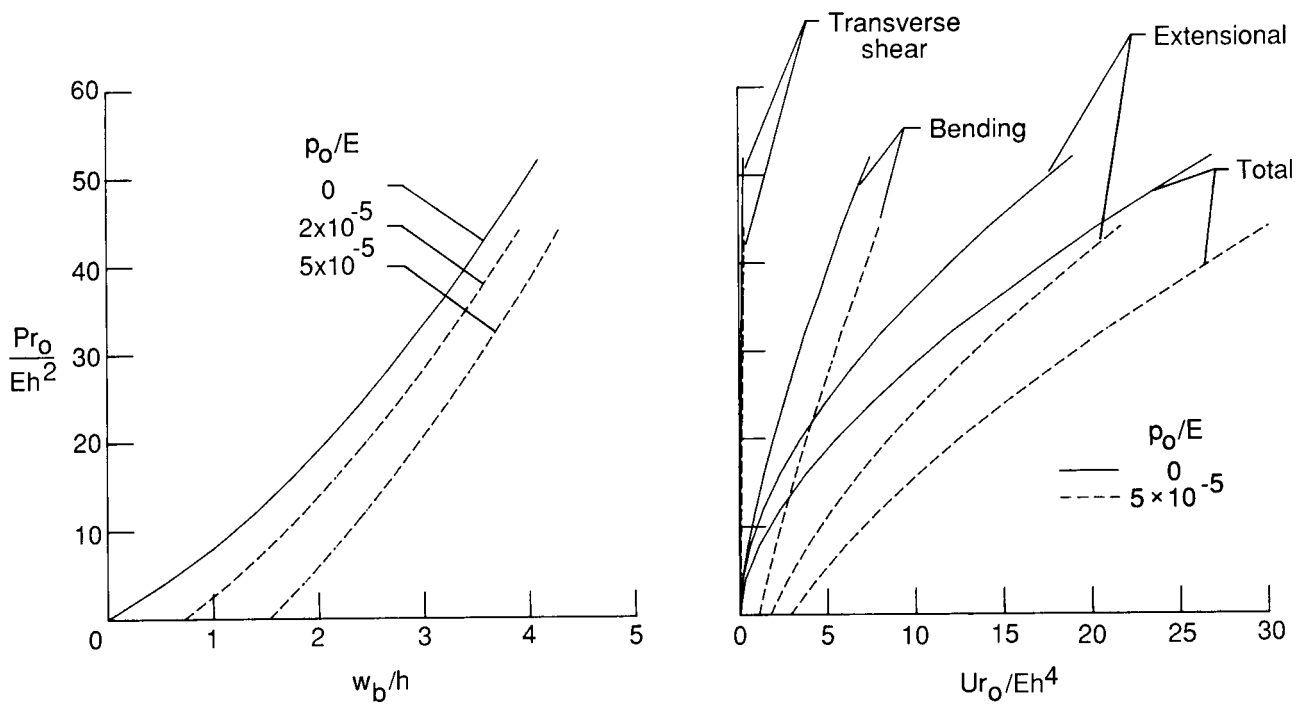

Figure 4. Variation of vertical displacement at the loaded end and total strain energy with loading for hemispherical shell.

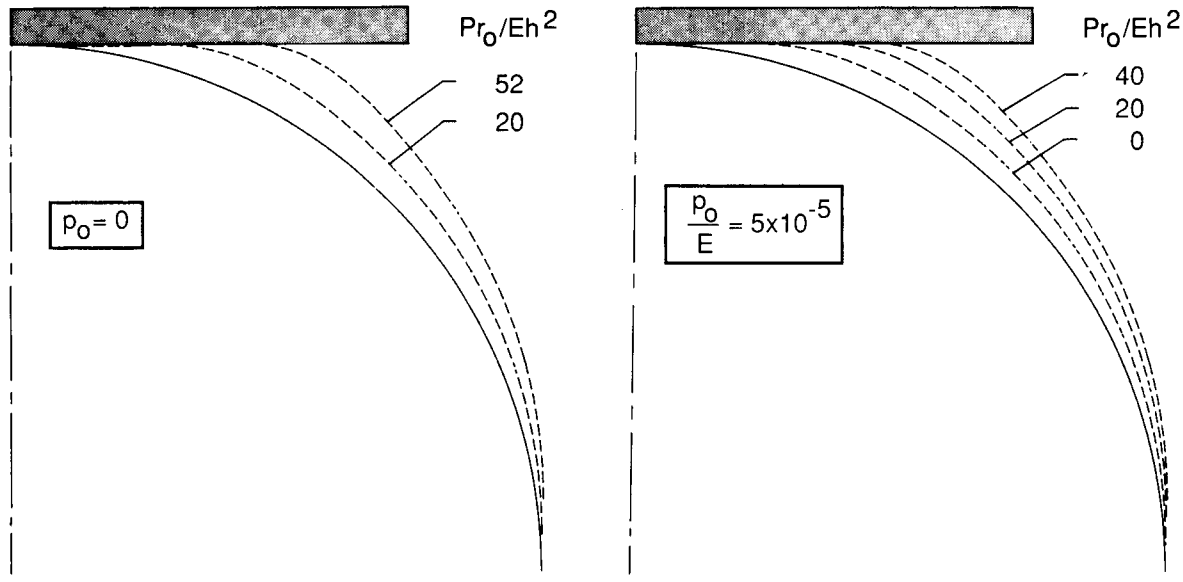

Figure 5. Deformed configurations of hemispherical shell.

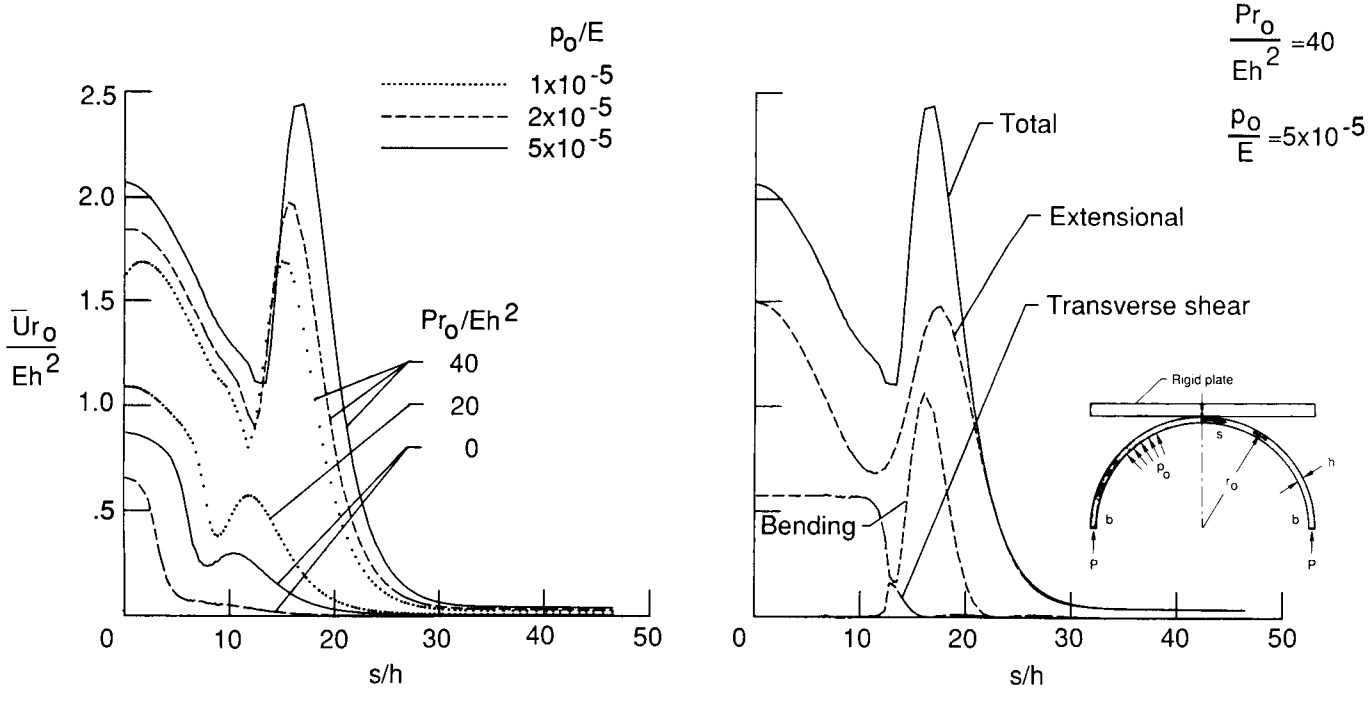

Figure 6. Distribution of strain energy densities along the meridian of hemispherical shell.

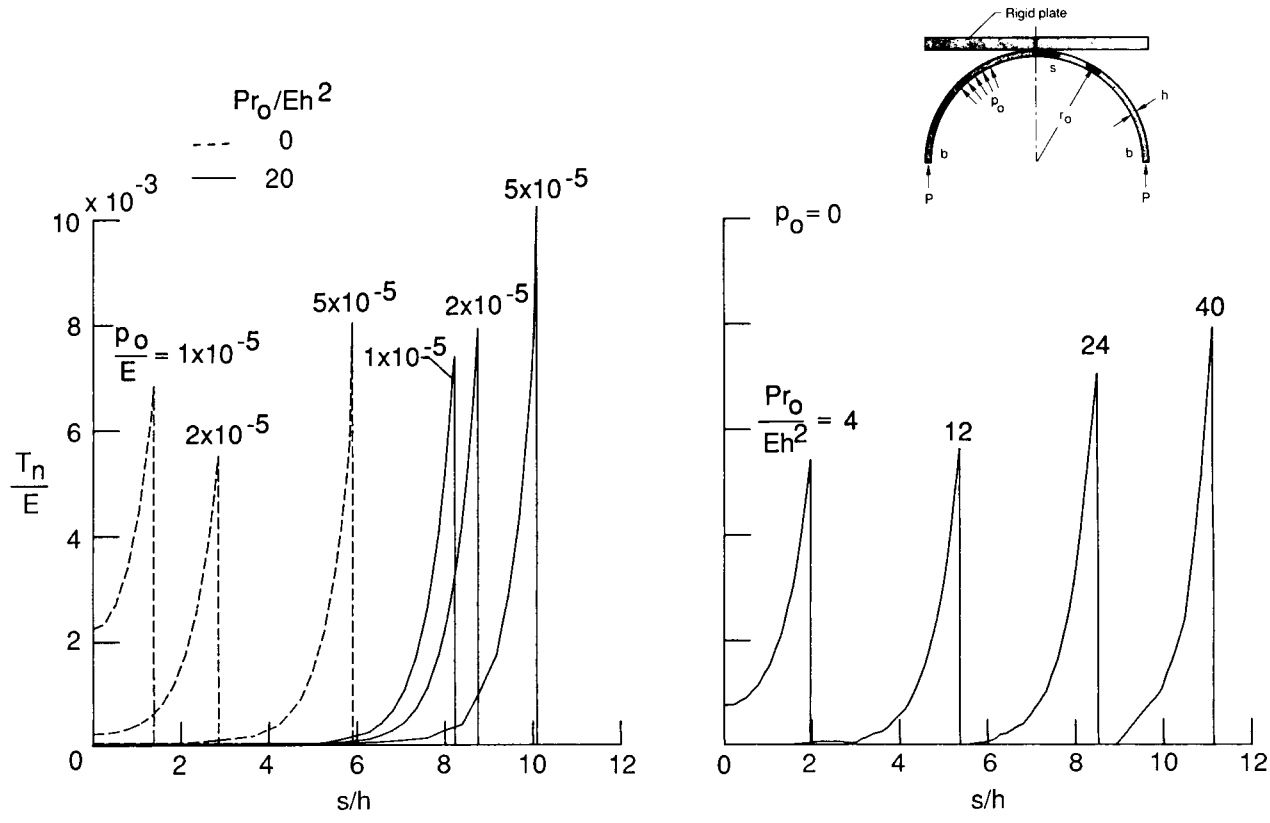

Figure 7. Distribution of contact pressures along the meridian of hemispherical shell.

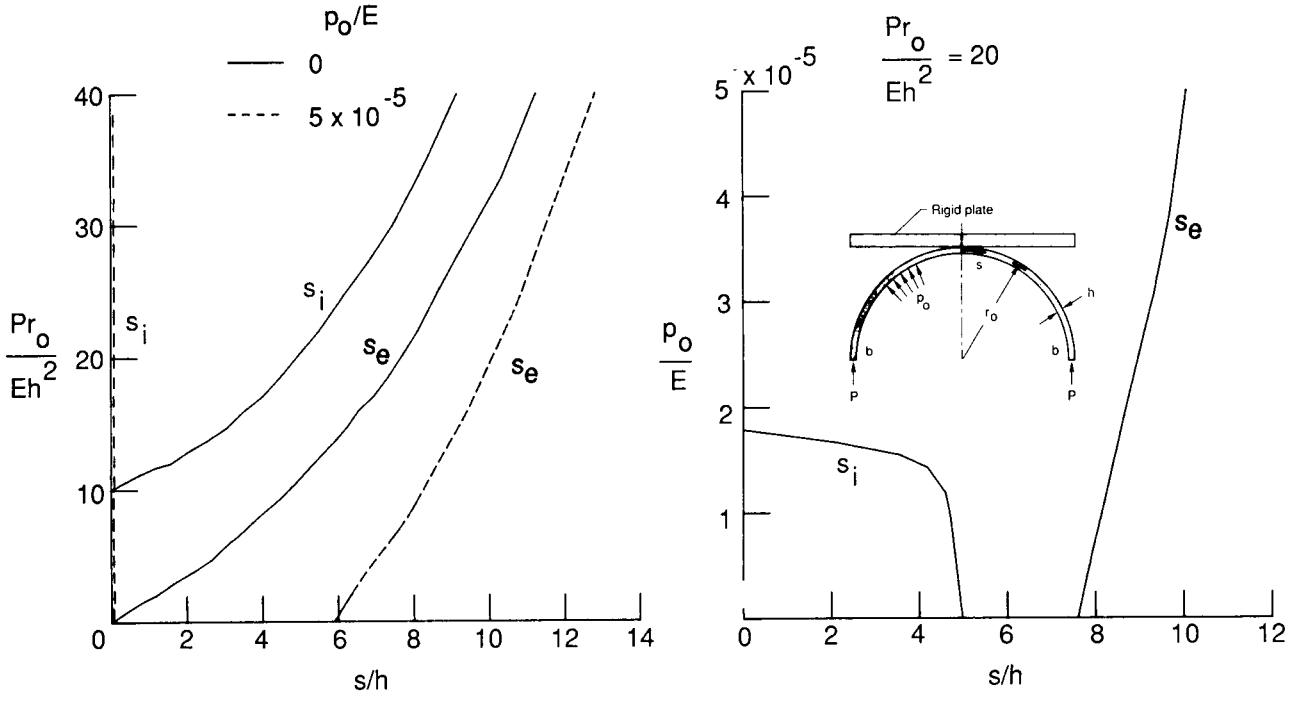

Figure 8. Variation of the contact region with loading for hemispherical shell. s_i and s_o refer to s-coordinates of initial and last contact points.

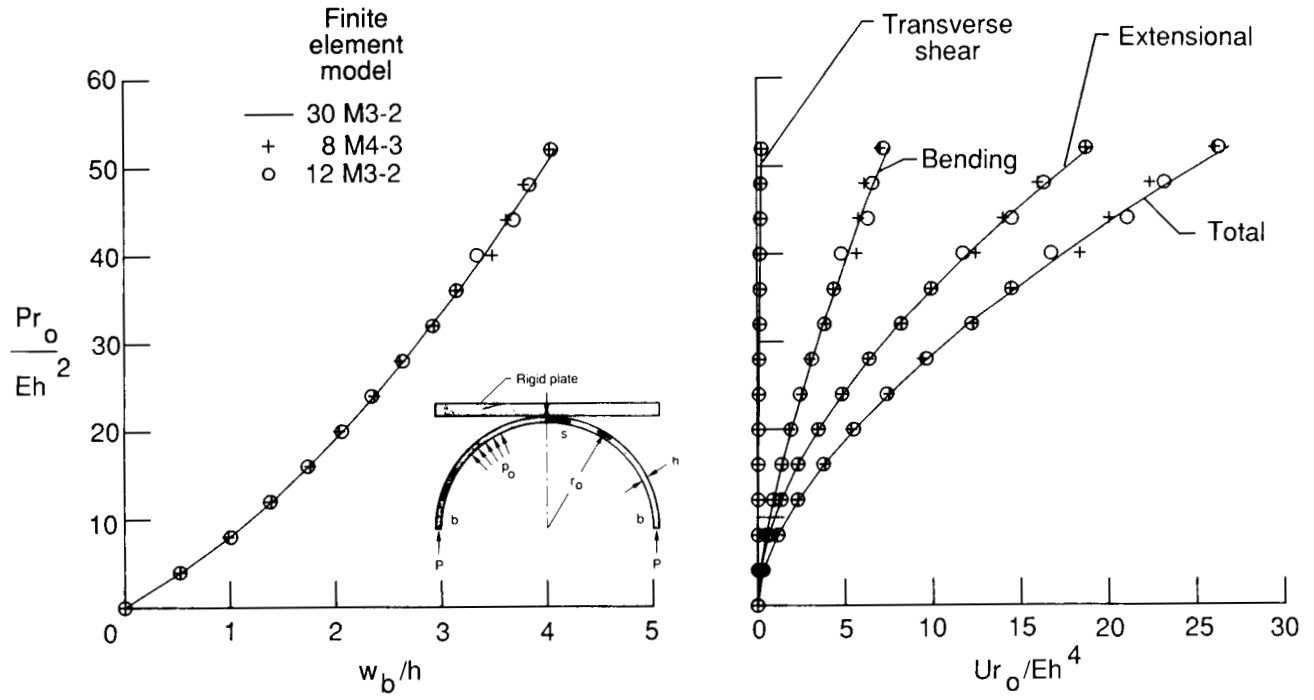

Figure 9. Accuracy of vertical displacement at loaded end and total strain energy obtained by mixed models of hemispherical shell. $p_o = 0$.

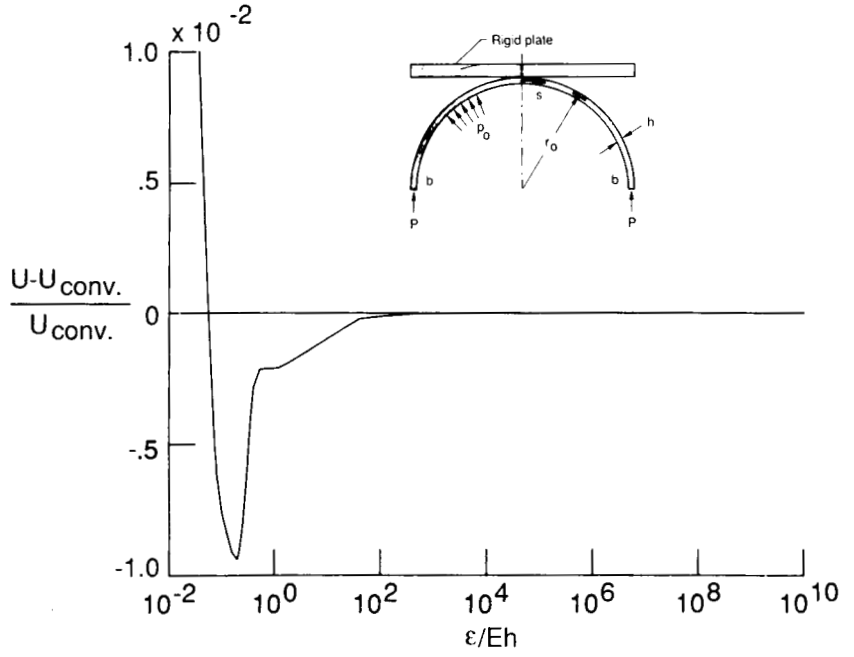

Figure 10. Effect of penalty parameter on accuracy of total strain energy for hemispherical shell. $Pr_o/Eh^2 = 2.0$; $p_o = 0$.

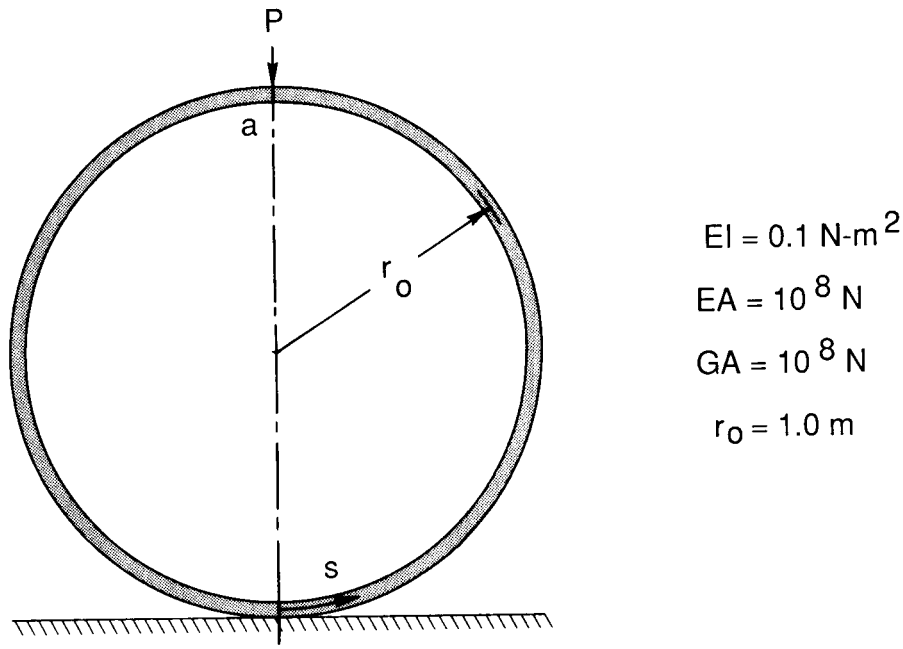

Figure 11. Circular ring pressed against rigid plate.

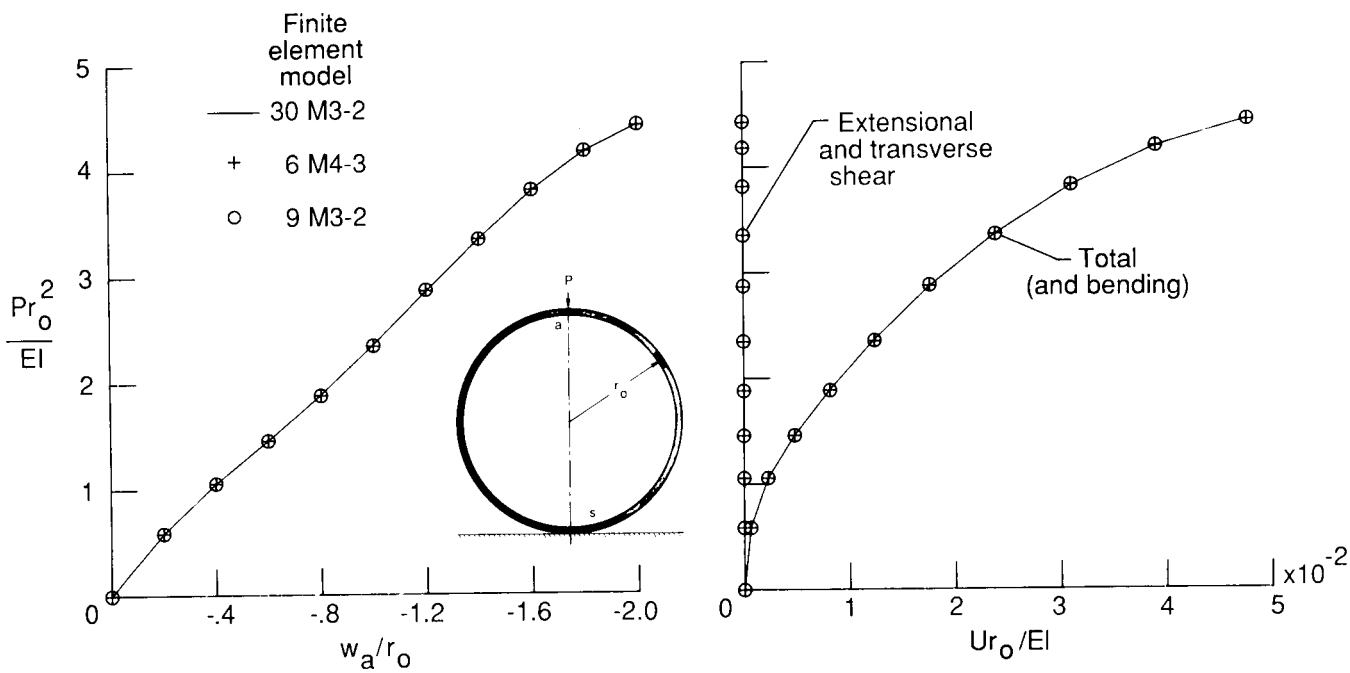

Figure 12. Variation of vertical displacement at the load point and total strain energy with loading for circular ring.

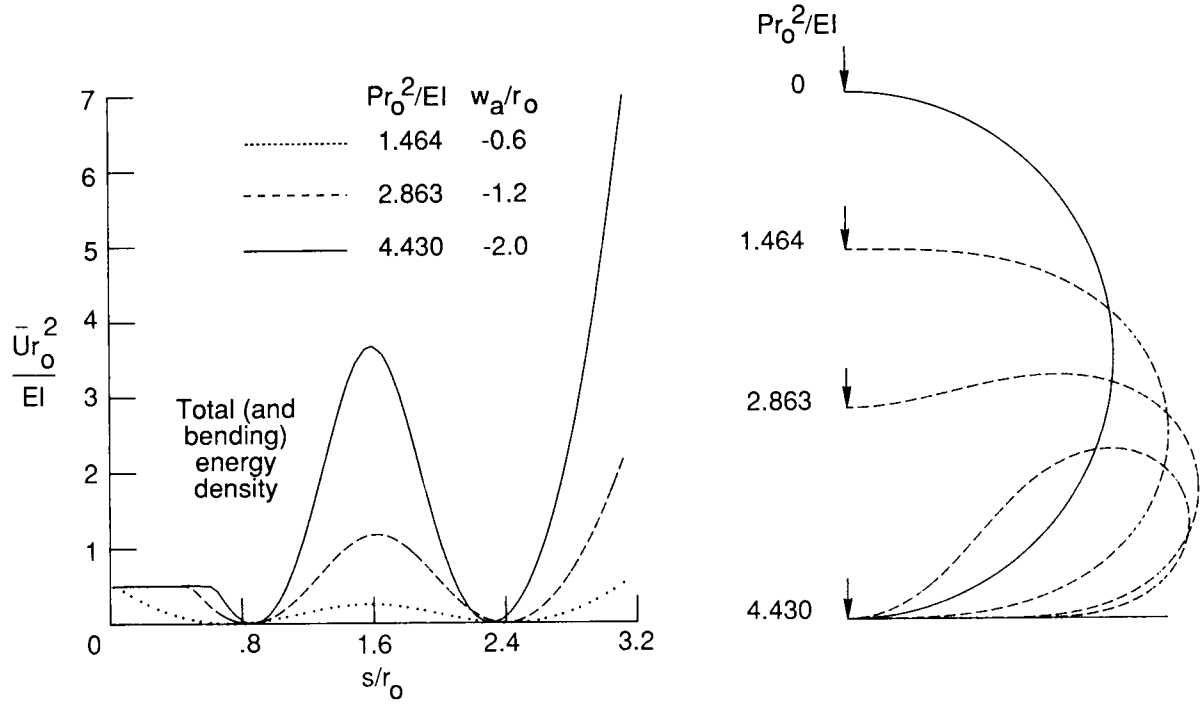

Figure 13. Deformed shapes and total strain energy density distributions for circular ring.

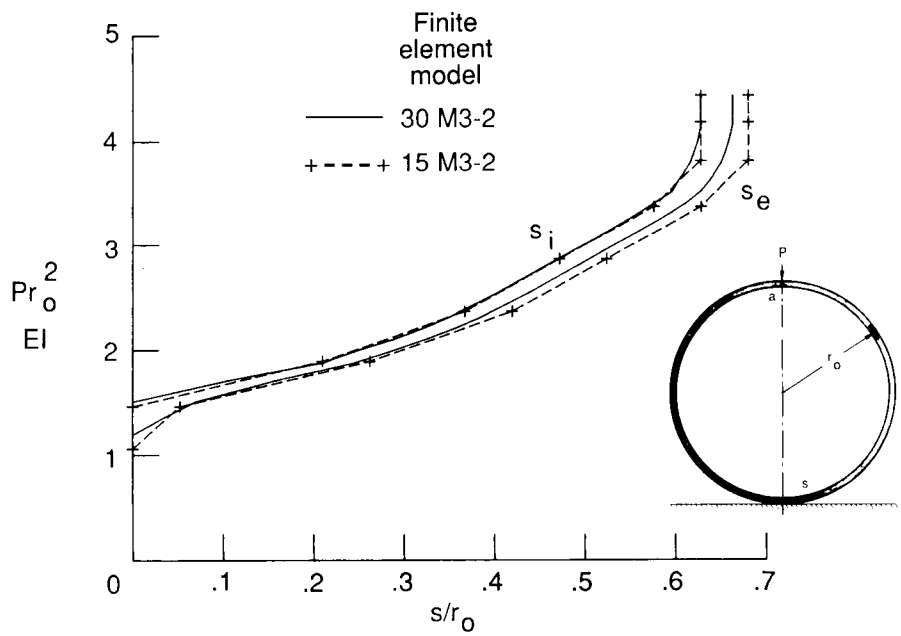

Figure 14. Variation of contact region with loading for circular ring. s_i and s_e refer to s-coordinates of initial and last contact points.

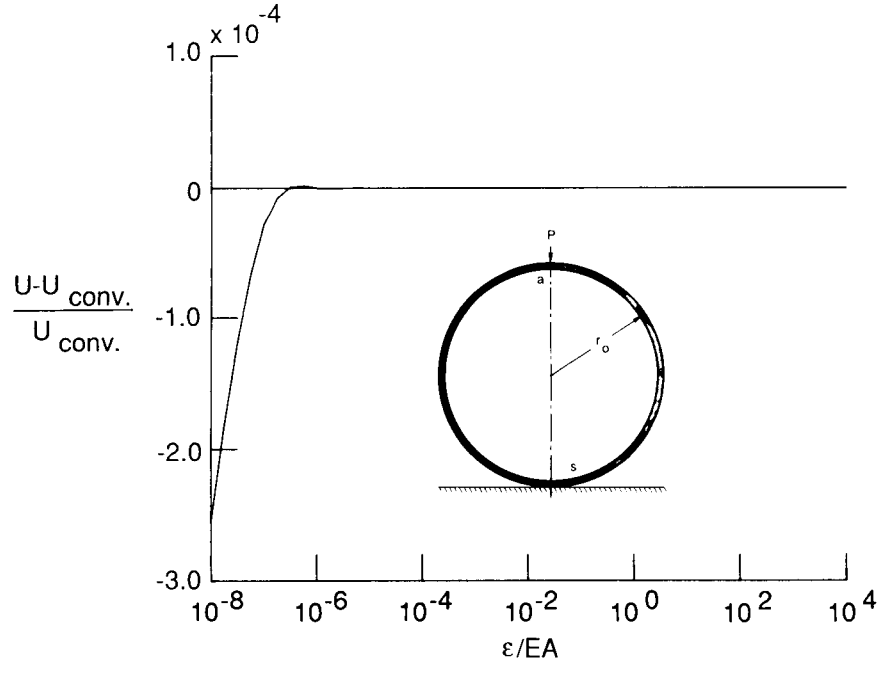

Figure 15. Effect of the magnitude of the penalty parameter on the accuracy of the total strain energy for the circular ring shown in figure 11.

NASA
National Aeronautics and Space Administration

Report Documentation Page

1. Report No.	2. Government Accession No.	3. Recipient's Catalog No.
NASA TP-2897		

4. Title and Subtitle	5. Report Date
Mixed Formulation for Frictionless Contact Problems	April 1989
	6. Performing Organization Code
7. Author(s)	8. Performing Organization Report No.
Ahmed K. Noor and Kyun O. Kim	L-16513
	10. Work Unit No.
9. Performing Organization Name and Address	505-63-41-02
NASA Langley Research Center Hampton, VA 23665-5225	11. Contract or Grant No.
	13. Type of Report and Period Covered
12. Sponsoring Agency Name and Address	Technical Paper
National Aeronautics and Space Administration Washington, DC 20546-0001	14. Sponsoring Agency Code

15. Supplementary Notes

Ahmed K. Noor and Kyun O. Kim: The George Washington University, Joint Institute for Advancement of Flight Sciences, Langley Research Center, Hampton, Virginia.

16. Abstract

Simple mixed finite element models and a computational procedure are presented for the solution of frictionless contact problems. The analytical formulation is based on a form of Reissner's large-rotation theory with the effects of transverse shear deformation included. The contact conditions are incorporated into the formulation by using a perturbed Lagrangian approach with the fundamental unknowns consisting of the internal forces (stress resultants), the generalized displacements, and the Lagrange multipliers associated with the contact conditions. The elemental arrays are obtained by using a modified form of the two-field Hellinger-Reissner mixed variational principle. The internal forces and the Lagrange multipliers are allowed to be discontinuous at interelement boundaries. The Newton-Raphson iterative scheme is used for solution of the nonlinear algebraic equations and for determination of the contact region and the contact pressures. Two numerical examples, axisymmetric deformations of a hemispherical shell and planar deformations of a circular ring, are presented. Both structures are pressed against a rigid plate. Detailed information about the response of both structures is presented. These examples demonstrate the high accuracy of the mixed models and the effectiveness of the computational procedure developed.

17. Key Words (Suggested by Authors(s))	18. Distribution Statement
Mixed finite elements Perturbed Lagrangian formulation Large rotations Frictionless contact Curved beams	Unclassified–Unlimited Subject Category 39

19. Security Classif. (of this report)	20. Security Classif. (of this page)	21. No. of Pages	22. Price
Unclassified	Unclassified	25	A03

For sale by the National Technical Information Service, Springfield, Virginia 22161-2171